**Data Repository materials.**

## 1. Methods.

**a. Determination of layer orientations.** 1m-resolution stereo terrain models were produced from High-Resolution Imaging Science Experiment (HiRISE) images, using the method of Kirk et al. (2008), and best-fitting planar layer orientations were calculated via linear regression of points along bedding contacts (procedure of Lewis et al., 2006). To confirm that our procedure is measuring layers within the mound, and is not biased by surficial weathering textures nor by the present-day slope, we made measurements around a small reentrant canyon incised into the SW corner of the Gale mound. Within this canyon, present-day slope dip direction varies through 360°, but as expected the measured layer orientations dip consistently (to the W).

**b. MarsWRF simulations of Gale Crater.** MarsWRF (Toigo et al., 2012) is the Mars version of planetWRF (Richardson et al., 2007), an extension of the widely-used Weather Research and Forecasting model. To produce the wind analysis shown in Figure DR1, MarsWRF was run as a global model at 2° resolution, with three increasingly high-resolution domains "nested" over Gale Crater to increase the resolution there to ~4 km. Each nested domain is both driven by its parent domain, and feeds information back to the parent domain, while also responding to surface variations (e.g. topography, albedo) at the higher resolution of the nest.

**c. Assessment of alternative mechanisms for producing outward dips.** Few geologic processes can produce primary outward dips of (3±2)° (Figures 1, 2). Spring mounds lack laterally continuous marker beds of the >10 km extent observed (Anderson & Bell, 2010). Preferential

dissolution, landsliding/halotectonics, post-impact mantle rebound, and lower-crustal flow can lead to postdepositional outward tilting. On Early Mars, isostatic compensation timescales are $<<10^6$ yr. In order for postdepositional mantle rebound to produce outward tilts, the mound must have accumulated at implausibly fast rates. Mars' crust is constrained to be $\lesssim$90 km thick at Gale's location (Nimmo & Stevenson, 2001), so lower-crustal flow beneath 155km-diameter Gale would have a geometry that would relax Gale Crater from the outside in, incompatible with simple outward tilting. Additionally, Gale is incompletely compensated (Konopliv et al., 2011) and postdates dichotomy-boundary faulting, so Gale postdates the era when Mars' lithosphere was warm enough for crustal flow to relax the dichotomy boundary and cause major deformation (Irwin & Watters, 2010). Any tectonic mechanism for the outward dips would correspond to ~3-4 km of floor uplift of originally horizontal layers. This is comparable to the depth of a fresh crater of this size and inconsistent with the current depth of the southern (mound-free) half of the crater if we make the reasonable approximation that wind cannot quickly erode basalt. Tectonic doming would put the mound's upper surface into extension and produce extensional faults (e.g., p.156 in Melosh, 2011), but these are not observed. Preferential dissolution leaves karstic depressions (Hovorka, 2000), which are not observed at Gale. Landsliding/halotectonics can produce deformed beds in layered sediments on Earth and Mars (e.g. Metz et al., 2010, Hudec & Jackson 2011). These sites show order-unity strain and contorted bedding, but the layers near the base of the mound show no evidence for large strains at kilometer scale, except for a possible late-stage landslide on the mound's north flank (Anderson & Bell, 2010).

**d. Scaling sediment transport.** Conservation of sediment (Anderson, 2008) in the atmospheric boundary-layer can be written as:

$$dz/dt = D - E = CWs - E$$

49 Here $C$ is volumetric sediment concentration, $Ws$ is settling velocity, and $E$ is the rate of sediment
50 pick-up from the bed. In aeolian transport of dry sand and alluvial-river transport, induration
51 processes are weak or absent and so the bed has negligible intergrain cohesion. $C$ tends to $E/Ws$
52 over a saturation length scale that is inversely proportional to $Ws$ (for $dz/dt > 0$) or $E$ (for $dz/dt < 0$).
53 This scale is typically short, e.g. ~1-20m, for the case of a saltating sand on Earth (Kok et al.,
54 2012). Our simplifying assumption that $D \neq f(x)$ and therefore $C \neq f(x)$ implies that this saturation
55 length scale is large compared to the morphodynamic feedback of interest. For the case of net
56 deposition ($dz/dt > 0$) this could correspond to settling-out of sediment stirred up by dust storms
57 (e.g. Vaughan et al., 2010). These events have characteristic length scales $>10^2$ km (Szwast et al.,
58 2006), larger than the scale of Gale's mound and justifying the approximation of uniform $D$. For
59 the case of net erosion ($dz/dt < 0$), small $E$ implies a detachment-limited system where sediment
60 has some cohesion. The necessary degree of induration is not large: for example, 6-10 mg/g
61 chloride salt increases the threshold wind stress for saltation by a factor of $e$ (Nickling, 1984). Fluid
62 pressure alone cannot abrade the bed, and the gain in entrained-particle mass from particle impact
63 equals the abrasion susceptibility, $\sim 2 \times 10^{-6}$ for basalt under modern Mars conditions (Bridges et al.,
64 2012) and generally $<<1$ for cohesive materials, preventing runaway adjustment of $C$ to $E/Ws$.
65 Detachment-limited erosion is clearly appropriate for slope-wind erosion on modern Mars (because
66 sediment mounds form yardangs and shed boulders, indicating that they are cohesive/indurated),
67 and is probably a better approximation to ancient erosion processes than transport-limitation (given
68 the evidence for ancient shallow diagenesis, and soil crusts; e.g., McLennan & Grotzinger, 2008).
69
70 **e. Reference parameter choices.** Coriolis forces are neglected because almost all sedimentary
71 rock mounds on Mars are equatorial (Kite et al., 2012). Additional numerical diffusivity at the $10^{-3}$
72 level is used to stabilize the solution. Analytic and experimental results show that in slope-wind

dominated landscapes, the strongest winds occur close to the steepest slopes (Manins & Sarford, 1987). $L$ will vary across Mars because of 3D topographic effects, and will vary in time because of changing atmospheric density. Ye et al. (1990) find $L \sim 20$km for Mars slopes with negligible geostrophic effects, and Eq. 49 in Magalhaes & Gierasch (1982) gives $L \sim 25$ km for Gale-relevant slopes. Simulations of gentle Mars slope winds strongly affected by planetary rotation suggest $L \sim$ 50-100 km (e.g., Savijärvi & Siili, 1993). Entrainment acts as a drag coefficient, ~0.02-0.05 for Gale-relevant slopes (e.g. Horst & Doran, 1986**)**, suggesting $L$ = 20-50 km for a 1km-thick cold boundary layer. Therefore we take $L \sim 10^{1\text{-}2}$ km to be reasonable, but with the expectation of significant $L/R$ variability, explored in the next section.

**2. Sensitivity tests: controls on mound growth and form.** To confirm that our results do not depend on idiosyncratic parameter choices, we carried out a parameter sweep in $\alpha$, $D'$, and $R/L$ (Figure DR2). Weak slope dependence ($\alpha = 0.05$) is sufficient to produce strata that dip toward the foot of the crater/canyon slope (like a sombrero hat). Similarly weak *negative* slope dependence ($\alpha = -0.05$) is sufficient to produce concave-up fill. At low $R/L$ (i.e., small craters) or at low $\alpha$, $D'$ controls overall mound shape and slope winds are unimportant. When $D'$ is high, layers fill the crater; when $D'$ is low, layers do not accumulate. When either $\alpha$ or $R/L$ or both are $\gtrsim 1$, slope-wind enhanced erosion and transport dominates the behavior. Thin layered crater floor deposits form at low $D'$, and large mounds at high $D'$. If $L$ is approximated as being constant across the planet, then $R/L$ is proportional to crater/canyon size. There is net aggradation everywhere for small $R/L$, although a small moat can form as a result of relatively low net aggradation near the crater wall. For larger $R/L$, moats form, and for the largest craters/canyons, multiple mounds can form eventually because slope winds break up the deposits. This is consistent with data, which suggest a maximum length scale for mounds (Figure DR3). Small exhumed craters in Meridiani show

97 concentric layering consistent with concave-up dips. Larger Meridiani craters, together with the
98 north polar ice mounds, show a simple single mound. Gale and Nicholson Craters, together with
99 the smaller Valles Marineris chasmata, show a single mound with an undulating top. The largest
100 canyon system on Mars (Ophir-Candor-Melas) shows multiple mounds per canyon. Gale-like
101 mounds (with erosion at both toe and the summit) are most likely for high $R/L$, high $\alpha$, and
102 intermediate $D'$ (high enough for some accumulation, not so high as to fill the crater; Figure DR2).
103 $U_o$ is set to zero in Figure 3. Sensitivity tests show that for a given $D'$, varying $U_o$ has little
104 effect on the pattern of erosion because spatial variations are still controlled by slope winds.
105 Equation (3) implies the approximation $E \sim \max(U)^{\alpha} \sim \sum U^{\alpha}$, which is true as $\alpha \rightarrow \infty$. To check
106 that this approximation does not affect conclusions for $\alpha$ = 3-4 (Kok et al., 2012), we ran a
107 parameter sweep with $E \sim (U_+^{\alpha} + U_-^{\alpha})$. For nominal parameters (Figure 3), this leads to only minor
108 changes in mound structure and stratigraphy (e.g., 6% reduction in mound height and <1% in
109 mound width at late time). For the parameter sweep as a whole, the change leads to a slight
110 widening of the regions where the mound does not nucleate or overspills the crater (changing the
111 outcome of 7 out of the 117 cases shown in Figure DR2). The approximation would be further
112 supported if (as is likely) there is a threshold $U$ below which erosion does not occur. If MSL shows
113 that persistent snow or ice was needed as a water source for layer cementation (Niles & Michalski,
114 2009; Kite et al., 2012), then additional terms will be required to track humidity and the drying
115 effect of föhn winds (e.g. Madeleine et al., 2012).
116 These sensitivity tests suggest that mounds are a generic outcome of steady uniform deposition
117 modified by slope-wind enhanced erosion and transport for reasonable Early Mars parameter
118 values.
119

**Data Repository References**


Anderson, R.S., 2008, The Little Book of Geomorphology: Exercising the Principle of Conservation, http://instaar.colorado.edu/~andersrs/The_little_book_010708_web.pdf

Horst, T. W., & Doran, J. C., 1986, Nocturnal drainage flow on simple slopes. *Boundary-Layer Meteorol.* 34, p. 263-286.

Hovorka, S. D., 2000, Understanding the processes of salt dissolution and subsidence in sinkholes and unusual subsidence over solution mined caverns and salt and potash mines, Technical Session: Solution Mining Research Institute Fall Meeting, p. 12–23, downloaded from http://www.beg.utexas.edu/environqlty/pdfs/hovorka-salt.pdf

Hudec, M.R., & Jackson, M.P.A., 2011, The salt mine : a digital atlas of salt tectonics. Austin, Tex: Jackson School of Geosciences, University of Texas at Austin.

Irwin, R. P., III, and T. R. Watters, 2010, Geology of the Martian crustal dichotomy boundary, *J. Geophys. Res*. 115, E11006, doi:10.1029/2010JE003658.

Konopliv, A.S. et al., 2011, Mars high resolution gravity fields from MRO, Mars seasonal gravity, and other dynamical parameters, *Icarus* 211, p. 401-428.

Madeleine, J.-B., Head, J. W., Spiga, A., Dickson, J. L., & Forget, F., 2012, A study of ice accumulation and stability in Martian craters under past orbital conditions using the LMD mesoscale model, *Lunar and Planet. Sci. Conf.* 43, abstract no. 1664.

Magalhaes, J., & Gierasch, P., 1982, A model of Martian slope winds: Implications for eolian transport, *J. Geophys. Res.* 87, p. 9975-9984.

Manins, P. C., & Sawford, B. L.,1987, A model of katabatic winds, *J. Atmos. Sci.* 36, 619-630.

Metz, J., Grotzinger, J., Okubo, C., & Milliken, R., 2010, Thin-skinned deformation of sedimentary rocks in Valles Marineris, Mars*, J. Geophys. Res*. 115, E11004.

Melosh, H.J., 2011, Planetary Surface Processes, Cambridge University Press.

144 Nickling, W.G., 1984, The stabilizing role of bonding agents on the entrainment of sediment by
145 wind. *Sedimentology* 31, 111-117. doi: 10.1111/j.1365-3091.1984.tb00726.x.
146 Nimmo, F., and Stevenson, D.J. 2001, Estimates of Martian crustal thickness from viscous
147 relaxation of topography, *J. Geophys. Res*. 106, 5085-5098, doi:10.1029/2000JE001331.
148 Richardson, M.I., Toigo, A.D., and Newman, C.E., 2007, PlanetWRF: A general purpose, local to
149 global numerical model for planetary atmospheric and climate dynamics, *J. Geophys. Res.* 112,
150 E09001.
151 Szwast, M., Richardson, M. and Vasavada, A., 2006, Surface dust redistribution on Mars as
152 observed by the Mars Global Surveyor and Viking orbiters. *J. Geophys. Res*. 111, E11008.
153 Savijärvi, H., and Siili, T., 1993, The Martian slope winds and the nocturnal PBL jet. *J. Atmos. Sci.*
154 50, p. 77-88.
155 Vaughan, A.F., et al., 2010. Pancam and Microscopic Imager observations of dust on the Spirit
156 Rover: Cleaning events, spectral properties, and aggregates, *Mars* 5, p. 129-145.
157 Ye, Z.J., Segal, M., & Pielke, R.A., 1990, A comparative study of daytime thermally induced
158 upslope flow on Mars and Earth. *J. Atmos. Sci.* 47, p. 612-628.

**Data Repository Table 1: Layer orientation measurements**

| Lat | Lon | Z (m) | Dip (°) | Dip Az (°) | HiRISE Image ID |
|---|---|---|---|---|---|
| -5.022347 | 138.394900 | -3263.1 | 3.53 | 30.68 | PSP_008437_1750 |
| -5.023877 | 138.392660 | -3201.9 | 2.52 | 62.01 | PSP_008437_1750 |
| -5.015876 | 138.386310 | -3216.9 | 2.1 | 94.68 | PSP_008437_1750 |
| -5.015508 | 138.387020 | -3201.4 | 7.31 | 41.72 | PSP_008437_1750 |
| -4.998358 | 138.391680 | -3554.2 | 2.06 | 54.81 | PSP_008437_1750 |
| -5.003035 | 138.387800 | -3429.9 | 0.43 | -21.29 | PSP_008437_1750 |
| -5.004517 | 138.379910 | -3425.8 | 5.04 | 89.54 | PSP_008437_1750 |
| -5.004179 | 138.379580 | -3434.5 | 3.79 | 70.24 | PSP_008437_1750 |
| -4.997492 | 138.392530 | -3583.8 | 4.65 | 51.98 | PSP_008437_1750 |
| -5.012374 | 138.396710 | -3421.5 | 4.14 | 47.28 | PSP_008437_1750 |
| -5.031424 | 138.395590 | -3290.1 | 4.07 | 40.92 | PSP_008437_1750 |
| -5.030106 | 138.396180 | -3308.2 | 2.55 | 76.18 | PSP_008437_1750 |
| -5.03171 | 138.393740 | -3260.1 | 3.24 | 43.31 | PSP_008437_1750 |
| -5.035189 | 138.392050 | -3176.3 | 2.07 | 75.25 | PSP_008437_1750 |
| -5.035062 | 138.391700 | -3173.3 | 2.21 | 86.77 | PSP_008437_1750 |
| -4.685812 | 137.494850 | -4098.5 | 3.34 | 148.1 | ESP_023957_1755 |
| -4.684778 | 137.491970 | -4103.8 | 3.98 | 174.47 | ESP_023957_1755 |
| -4.689331 | 137.480520 | -4101.3 | 6.06 | 132.82 | ESP_023957_1755 |
| -4.659387 | 137.533150 | -4120.3 | 6.48 | 114.03 | ESP_023957_1755 |
| -4.65886 | 137.537400 | -4108.2 | 0.5 | 13.56 | ESP_023957_1755 |
| -4.662119 | 137.535520 | -4073.1 | 3.9 | -149.05 | ESP_023957_1755 |
| -4.664102 | 137.525670 | -4127.1 | 7.16 | 130.19 | ESP_023957_1755 |
| -4.663656 | 137.524870 | -4138.3 | 4.83 | 152.05 | ESP_023957_1755 |
| -4.665528 | 137.526530 | -4101.2 | 4.59 | -153.08 | ESP_023957_1755 |
| -4.676802 | 137.506150 | -4083.2 | 2.32 | 83.97 | ESP_023957_1755 |
| -4.672137 | 137.510280 | -4128 | 3.24 | 91.62 | ESP_023957_1755 |
| -4.871501 | 137.270980 | -3849.6 | 1.09 | 10.19 | PSP_001488_1750 |
| -4.871837 | 137.266710 | -3857.7 | 5.19 | 85.97 | PSP_001488_1750 |
| -4.872691 | 137.270730 | -3833.2 | 2.61 | -51.44 | PSP_001488_1750 |
| -4.917952 | 137.284340 | -3513.9 | 6.78 | 136.55 | PSP_001488_1750 |
| -4.831027 | 137.330630 | -3768.9 | 2.16 | 140.09 | PSP_001488_1750 |
| -4.828565 | 137.330360 | -3792.5 | 2.65 | 143.84 | PSP_001488_1750 |
| -4.846642 | 137.303380 | -3802.8 | 4.38 | 124.94 | PSP_001488_1750 |
| -4.845724 | 137.303070 | -3815.7 | 4.51 | 111.27 | PSP_001488_1750 |
| -4.845501 | 137.304420 | -3799.2 | 2.34 | 79.11 | PSP_001488_1750 |
| -4.863885 | 137.332420 | -3507.1 | 2.04 | 132.56 | PSP_001488_1750 |
| -4.93696 | 137.311640 | -3278.4 | 3.74 | 129.01 | PSP_001488_1750 |
| -4.938936 | 137.309840 | -3287.6 | 4.46 | 119.79 | PSP_001488_1750 |
| -4.920126 | 137.322160 | -3290.9 | 1.79 | 134.69 | PSP_001488_1750 |
| -4.922859 | 137.317020 | -3306.6 | 4.2 | 160.7 | PSP_001488_1750 |
| -4.901912 | 137.338220 | -3265.6 | 4.87 | -174.83 | PSP_001488_1750 |

| | | | | | |
|---|---|---|---|---|---|
| -4.892401 | 137.332800 | -3389.9 | 6.71 | 117.93 | PSP_001488_1750 |
| -4.863151 | 137.342100 | -3464.4 | 5.66 | 105.35 | PSP_001488_1750 |
| -4.779928 | 137.409690 | -3656.9 | 3.69 | 167.09 | PSP_009149_1750 |
| -4.777029 | 137.405330 | -3736.8 | 2.13 | 168.14 | PSP_009149_1750 |
| -4.75303 | 137.438670 | -3810.7 | 6.07 | 128.67 | PSP_009149_1750 |
| -4.752131 | 137.438100 | -3823.7 | 5.92 | 123.62 | PSP_009149_1750 |
| -5.348423 | 137.227120 | -2745.9 | 2.68 | 154.47 | ESP_012907_1745 |
| -5.348098 | 137.227470 | -2757.1 | 2.32 | 144.88 | ESP_012907_1745 |
| -5.341016 | 137.209820 | -2891.2 | 2.58 | 135.34 | ESP_012907_1745 |
| -5.337968 | 137.210930 | -2796.8 | 4.54 | 151.03 | ESP_012907_1745 |
| -5.377012 | 137.207730 | -2879.1 | 1.63 | 165.41 | ESP_012907_1745 |
| -5.384663 | 137.190610 | -3005.3 | 4.73 | 156.7 | ESP_012907_1745 |
| -5.413138 | 137.185680 | -2848.5 | 4.57 | 133.72 | ESP_012907_1745 |
| -5.40772 | 137.197850 | -2779.3 | 4.05 | 158.01 | ESP_012907_1745 |
| -5.392686 | 137.208330 | -2756.1 | 10.83 | 163.21 | ESP_012907_1745 |
| -5.371398 | 137.174520 | -3359.7 | 6.02 | 159.19 | ESP_012907_1745 |
| -5.342561 | 137.176890 | -3130.9 | 6.76 | 160.11 | ESP_012907_1745 |
| -5.458482 | 137.183800 | -2752.8 | 2.49 | 142.76 | ESP_012907_1745 |
| -5.459221 | 137.188840 | -2674.5 | 3.58 | 162.7 | ESP_012907_1745 |
| -5.460307 | 137.188440 | -2696.5 | 3.97 | 166.94 | ESP_012907_1745 |
| -5.392535 | 137.196770 | -2848.2 | 2.48 | 170.27 | ESP_012907_1745 |
| -5.390379 | 137.195930 | -2898.2 | 3.04 | 156.57 | ESP_012907_1745 |
| -5.390219 | 137.191070 | -2988.8 | 2.6 | 144.9 | ESP_012907_1745 |
| -5.411481 | 137.194250 | -2811.9 | 2.09 | 146.02 | ESP_012907_1745 |
| -5.623904 | 138.328080 | -2971.2 | 1.74 | -43.56 | ESP_014186_1745 |
| -5.627848 | 138.337550 | -3000.2 | 2.17 | -71.76 | ESP_014186_1745 |
| -5.598681 | 138.339300 | -2856.2 | 1.26 | 116.18 | ESP_014186_1745 |
| -5.584488 | 138.338620 | -2705.9 | 2.25 | -69.68 | ESP_014186_1745 |
| -5.584654 | 138.354940 | -2710 | 2.45 | -82.66 | ESP_014186_1745 |
| -5.605716 | 138.360870 | -2907.7 | 0.3 | -175.97 | ESP_014186_1745 |
| -5.570108 | 138.366460 | -2674.6 | 5.23 | -61.61 | ESP_014186_1745 |
| -5.572424 | 138.360000 | -2589.6 | 2.17 | -86.77 | ESP_014186_1745 |
| -5.588566 | 138.326250 | -2685.2 | 2.6 | -27.67 | ESP_014186_1745 |
| -5.580666 | 138.333270 | -2681.5 | 1.76 | -81.46 | ESP_014186_1745 |
| -5.534321 | 138.325470 | -2424.8 | 4.35 | -117.38 | ESP_014186_1745 |
| -5.542813 | 138.327860 | -2454.8 | 3.37 | -104.06 | ESP_014186_1745 |
| -5.573589 | 138.289520 | -2658.6 | 2.2 | -115.72 | ESP_014186_1745 |
| -5.566658 | 138.288200 | -2644.4 | 1.15 | 74.46 | ESP_014186_1745 |
| -5.581102 | 138.309950 | -2667.3 | 1.06 | -65.97 | ESP_014186_1745 |

160

**Data Repository Figure Captions**

**Figure DR1.** Annual maximum wind speed (m/s) within Gale Crater from MarsWRF simulations, showing that the strongest winds within the crater are associated with steep slopes. Black topography contours are spaced at 500m intervals. The winds are extrapolated to 1.5m above the surface using boundary layer similarity theory (the lowest model layer is at ~9m above the surface).

**Figure DR2.** Overall growth and form of sedimentary mounds – results from a model parameter sweep varying $R/L$ and $D'$, with fixed $\alpha = 3$. Black square corresponds to the results shown in more detail in Figure 3. Symbols correspond to the overall results:– no net accumulation of sediment anywhere (blue open circles); sediment overtops crater/canyon (red filled circles); mound forms and remains within crater (green symbols). Green filled circles correspond to outcomes where layers are exposed at both the toe and the summit of mound, similar to Gale.

**Figure DR3.** Width of largest mound does not keep pace with increasing crater/canyon width, suggesting a length threshold beyond which slope winds break up mounds. Blue dots correspond to nonpolar crater data, red squares correspond to canyon data, and green dots correspond to polar ice mound data. Gray vertical lines show range of uncertainty in largest-mound width for Valles Marineris canyons. Blue dot adjacent to "G" corresponds to Gale Crater. Craters smaller than 10km were measured using Context Camera (CTX) or HiRISE images. All other craters, canyons and mounds were measured using the Thermal Emission Imaging System (THEMIS) global day infrared mosaic on a Mars Orbiter Laser Altimeter (MOLA) base. Width is defined as polygon area divided by the longest straight-line length that can be contained within that polygon.

Figure DR1

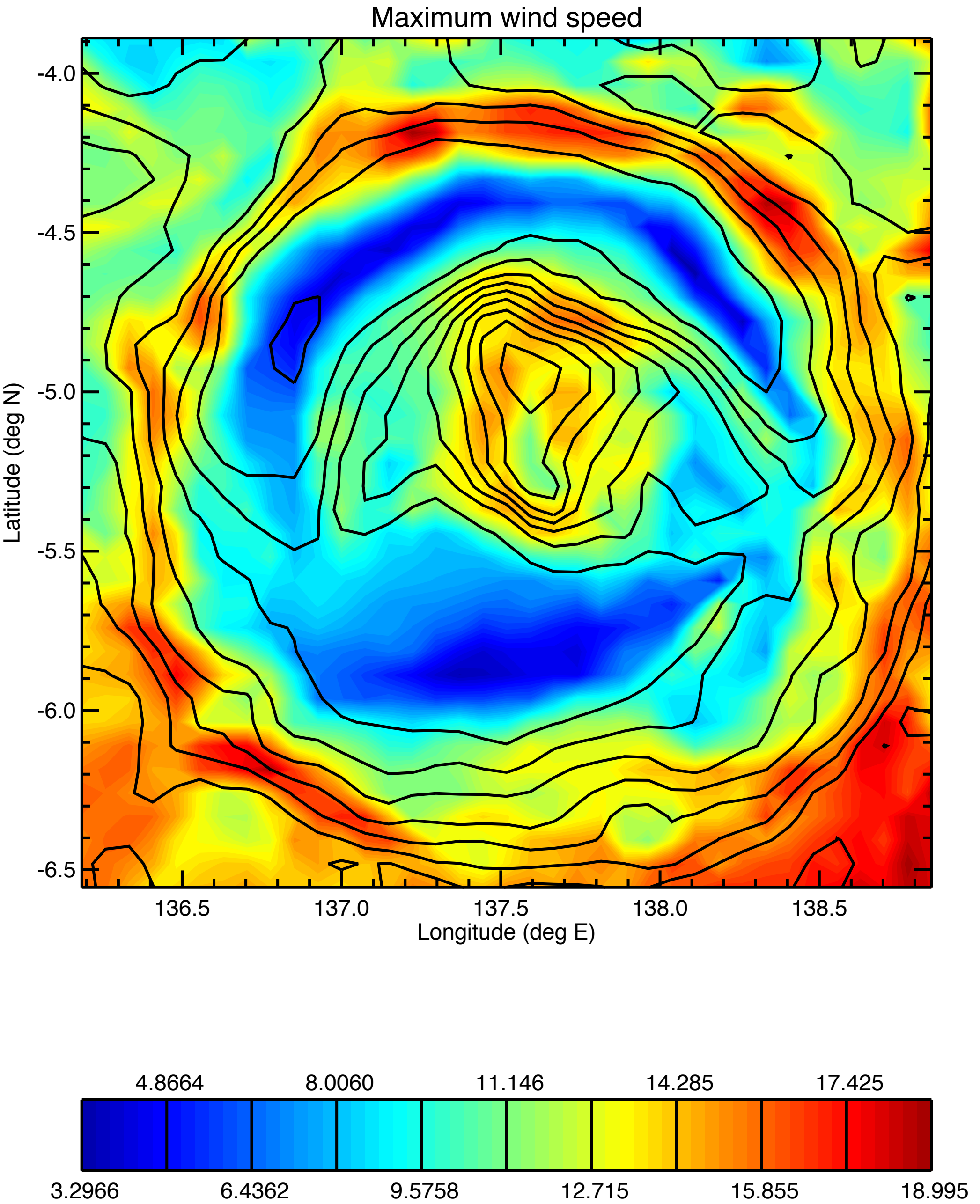
Maximum wind speed
-4.0
-4.5
-5.0
-5.5
-6.0
-6.5
Latitude (deg N)
136.5
137.0
137.5
138.0
138.5
Longitude (deg E)
4.8664
8.0060
11.146
14.285
17.425
3.2966
6.4362
9.5758
12.715
15.855
18.995

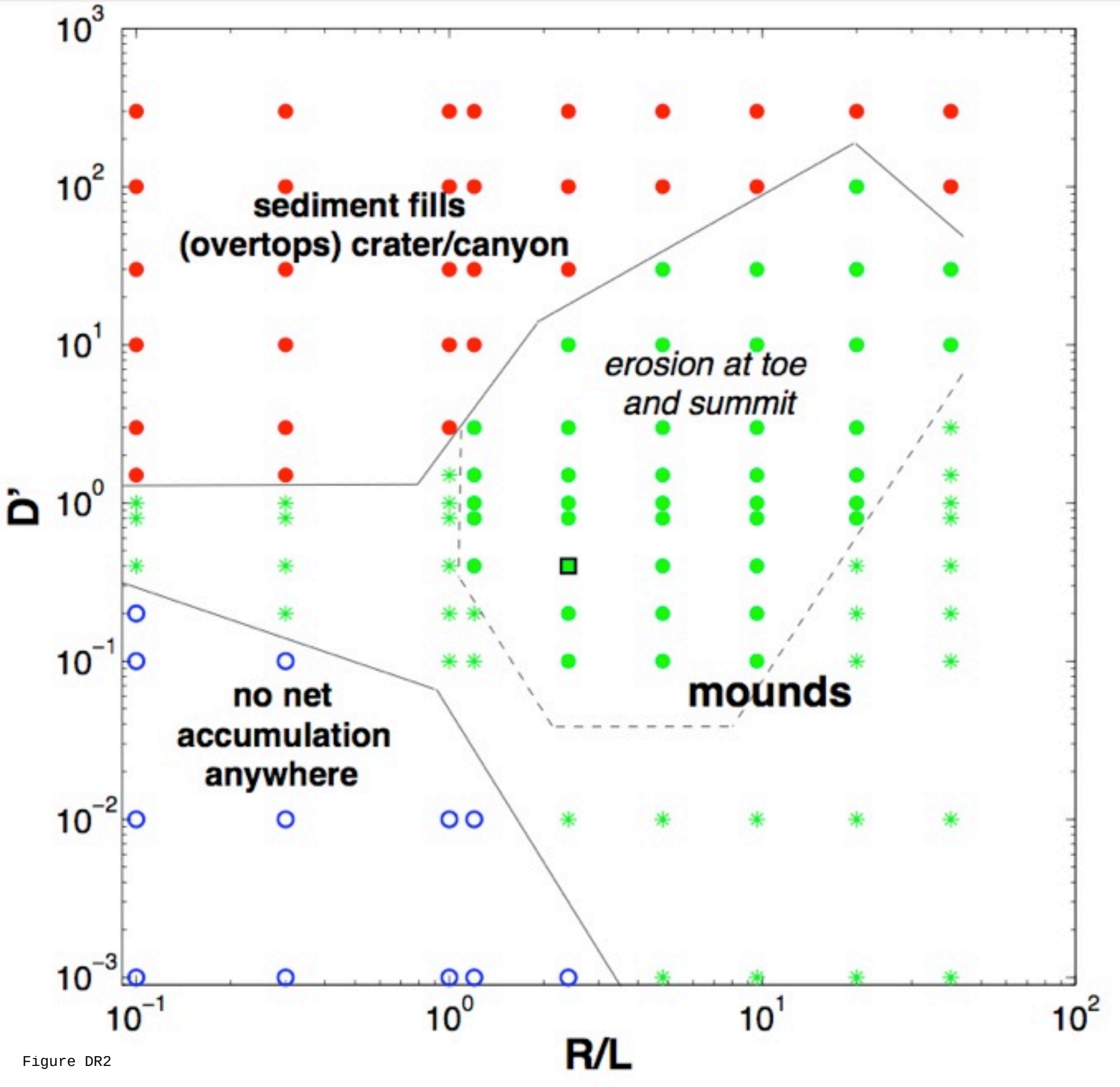
sediment fills
(overtops) crater/canyon
erosion at toe
and summit
mounds
no net
accumulation
anywhere
D'
R/L
$10^3$
$10^2$
$10^1$
$10^0$
$10^{-1}$
$10^{-2}$
$10^{-3}$
$10^{-1}$
$10^0$
$10^1$
$10^2$

Figure DR2

Figure DR3

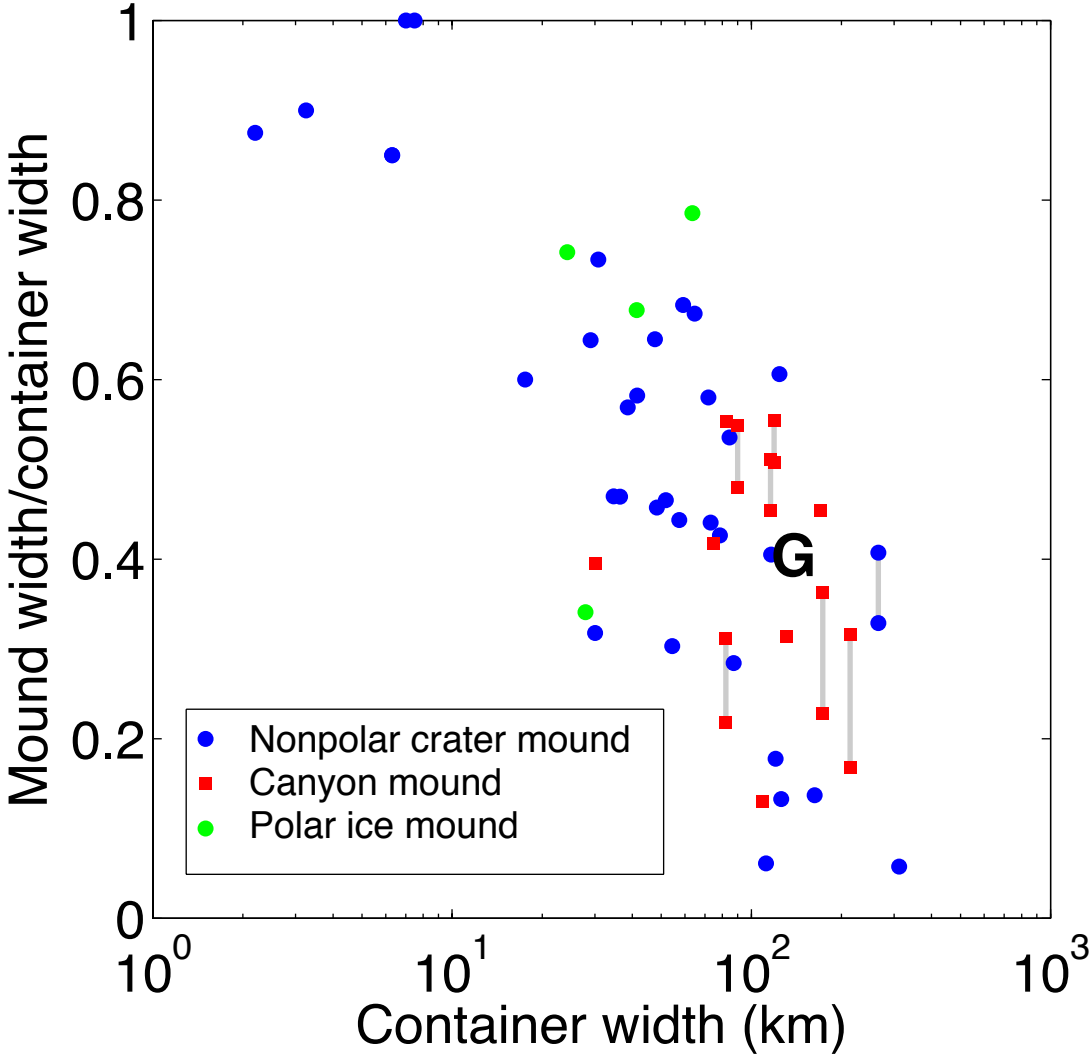
Mound width/container width
Container width (km)
1
0.8
0.6
0.4
0.2
0
$10^0$
$10^1$
$10^2$
$10^3$
G
Nonpolar crater mound
Canyon mound
Polar ice mound